Gold/mesoporous silica-fiber core-shell hybrid nanostructure: a potential electron transfer mediator in a bio-electrochemical system†

Haigang Kang, Yihua Zhu,* Xiaoling Yang, Jianhua Shen, Cheng Chen and Chunzhong Li

Received (in Victoria, Australia) 4th February 2010, Accepted 3rd May 2010
DOI: 10.1039/c0nj00094a

Mesostructured silica fibers synthesized by electrospinning silica sol were used as templates for the assembly of gold nanoparticles and the formation of continuous gold shells along the fiber axis. Dense and uniform spherical gold nanoparticles were formed by *in situ* reduction of hydrochloroauric acid absorbed on self-assembled polyelectrolyte film of silica fiber surface. The gold-seeded silica fibers were further coated by continuous gold shells *via* solution-phase reduction of an appropriate metal ion in PVP solution. The thickness and morphology of gold shell could be tailored by the molar ratio of repeating units of PVP to gold ions (R) and growth time. Experimental results showed that low R tended to form a thick gold layer with sharp tips, whereas high R favored obtaining thin and uniform Au shell. The SiO_2@Au fiber hybrid nanostructures are further used as substrates for fabrication of a glucose biosensor, which exhibited excellent bio-electrochemical activity with high sensitivity and rapid response. These hybrid nanostructures are, therefore, regard as molecule wires for potential application in highly sensitive chemical or biological sensors.

1. Introduction

A significant step after the remarkable success in growing single-component nanocrystals is the preparation of nanostructures that are composed of discrete domains of different materials. The attraction of multicomponent nanostructures is that multiple functions can be integrated into one system for specific applications.[1–8] Moreover, the interactions between nanoscale-spaced components can greatly improve the overall application performance of the nanostructured system and even generate new synergetic properties. For example, in noble meta-semiconductor nanostructures, metallic ingredients can improve the charge separation[9,10] and enhance light absorption in semiconductors.[11,12] Both effects can increase the photocatalytic and light-harvesting efficiencies of semiconductors. In the past several decades, gold nanoparticles have attracted strong interest in the fundamental sciences and have been widely investigated for their potential uses in a range of technological and biological applications including. For example, potential uses include photothermal therapies,[13,14] targeted labeling,[15] surface-enhanced spectroscopies,[16] biosensors,[17] biological detection,[18] and chemical catalysis.[19] Due to its nontoxic nature, optical transparency, chemical inertness, thermal stability, high biocompatibility, adjustable pore diameter, and very high specific surface area with abundant Si–OH bonds on the surface, mesoporous silica has been widely used in coating or supporting heterogeneous component materials,[20] and applied in many fields including catalysis,[21,22] ion detection,[23] and sensors. From these viewpoints, the combination of mesoporous silica and noble metals in one nanocomposite would form a unique multifunctional material.

Since the pioneering silica-coated gold nanoparticles were first synthesized by the Mulvaney group in 1996,[24] they have been intensively studied due to their feasible manipulation and extensive application in biosensors or non-linear optical materials. This kind of spherical core–shell colloid could be applied to photonic crystals and plasmonic waveguides to act as an optical instrument. By changing the thickness of the silica shell and the diameter of the gold core, direct control of the effectiveness of the optical instrument would become possible.[25] Au@SiO_2 nanoparticles have well-established chemical properties that allow surface modification with various functional groups (*e.g.*, amine, thiol, carboxyl, methyl and methacrylate). These surface functionalized Au@SiO_2 nanoparticles can be further modified with biomolecules for biological applications.[26] Considerable studies about core-shell Au@SiO_2 nanoparticles prepared by the liquid phase procedures have been made. General synthesis methods include the following three steps: (1) modification of the gold nanoparticles surfaces to make them vitreophilic by using silane coupling reagent as primer, such as APTS,[27] APTMOS,[28] (2) slow silica deposition in water from a sodium silicate solution and (3) extensive growth of silica shells through sol–gel reaction of TEOS in ethanol and ammonia mixtures.[29]

As for SiO_2@Au core-shell hybrid, synthesis can be achieved in two ways, one is that metal particles are synthesized or deposited directly on the core surface without

Key Laboratory for Ultrafine Materials of Ministry of Education, East China University of Science and Technology, Shanghai 200237, China. E-mail: yhzhu@ecust.edu.cn; Fax: +86 2164250624; Tel: +86 2164250624

† Electronic supplementary information (ESI) available: Infrared spectra, DTG and TGA, N_2 adsorption–desorption isotherm and TEM images. See DOI: 10.1039/c0nj00094a

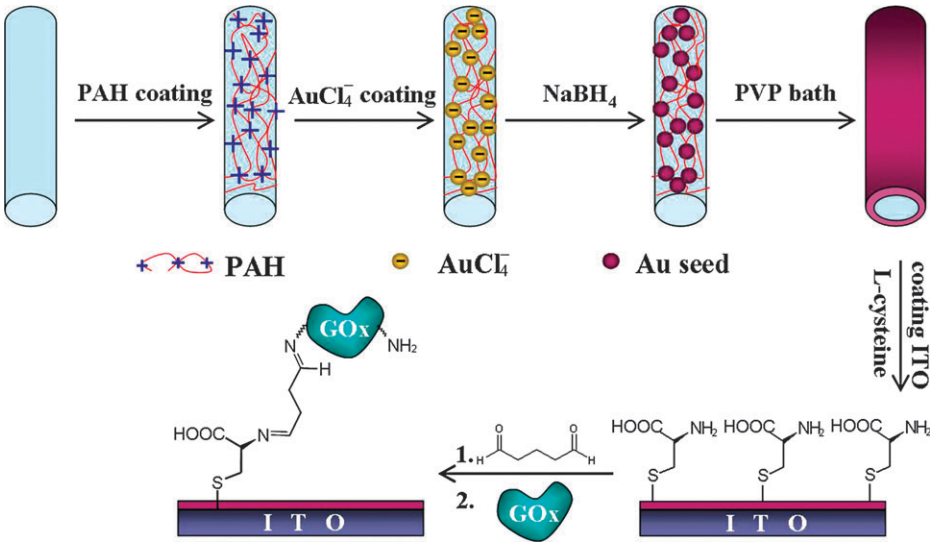

Scheme 1 Schematic diagram illustrates of the formation of SiO_2@Au core-shell fibers and immobilization of GOx.

pretreatment. The other is to modify or functionalize the core surface before adding the dielectric colloidal core into metal nanoparticles solution or metal salt solution. Although those methods work well, there are two drawbacks: one is the tedious procedure in which gold and silica nanoparticles need to be presynthesized respectively and then bridged by silane coupling agent; the other is the resulting low or nonuniform particle densities in the shell layer.[30] The layer-by-layer (LBL) assembly is an efficient and simple method to construct high-quality and uniform coatings on the substrates, which varied from macroscopically platform charged surfaces to micro-metre- and submicrometre-sized, charged colloidal particles and even nanoparticles.[31,32] Dong *et al.*[2] used polyelectrolyte, PMAA/PEI, to modify the Fe_3O_4 particles through the LBL method to assemble large numbers of gold seeds. Highly rough Fe_3O_4 core/Au shell particles with nanoscale roughness and gaps were formed after the final reduction with hydroxylamine hydrochloride. Logar's group fabricated self-assembled multi-layer thin films by the sequential adsorption of appositively charged polyelectrolytes, which were used as a template for the *in situ* nucleation and growth of silver (Ag) nanoparticles.[33] With this synthesis methodology a uniform distribution of spherical Ag nanoparticles in a polymer matrix was obtained. Diaz and co-workers designed bifunctional gold-coated magnetic silica spheres.[34] First, three layers of polyelectrolytes with a positive charge were adsorbed onto the magnetic silica spheres, and then the continuous deposition of gold seeds created an outer nanoparticulate shell.

However, study related to gold nanoparticle-decorated silica fibers or core-shell hybrid is seldom reported. Only Wang *et al.* used silica nanofibers synthesized with the structure-directing agent (cetyltrimethylammonium bromide) in HBr solutions as templates for the assembly of Au and Ag nanoparticles and the formation of thin gold shells along the fiber axis.[35] Guo *et al.* reported the synthesis of tubular gold and silver nano-shells on silica nanowire templates in solution.[36]

Although core–shell nanostructures have attracted much interest due to the combination of different properties in one particle constructed of different chemical components, almost all interest is presently focused on the optical characteristics,[37,38] while the bio-electrochemical properties in biohybrid systems, such as biocatalytical activity for immobilized enzyme in amperometric biosensors, have not been reported. Therefore, herein we investigated the specific bioelectrochemical property of fibrous SiO_2@Au core-shell structure applied in a glucose biosensor, because in comparison with the sphere colloid, the large surface area of the hybrid fibers favors immobilizing more enzyme molecules and three-dimensional network based on the interconnected gold-coated silica fibers will enhance the electron exchange of proteins with electrodes. Moreover, Wang's group has demonstrated that the fibrous morphology seems to exhibit higher thermal and electric conductivities than others, such as plates or spheres.[39,40] Taking these advantages into account, electrospun fibers are exploited for diverse applications, such as optoelectronics,[41] sensor technology,[42] drug delivery.[43,44]

Motivated by these advantages, in this paper, we introduced gold seeds onto fiber surface by *in situ* reduction of $AuCl_4^{-1}$ absorbed on self-assembled polyelectrolyte film of electrospun silica fiber surface. This seed-mediated growth is further used to form continuous gold shells around the silica nanofibers. The integrity and thickness of the gold shell could be tuned by varying the reaction time in the constant amount of seeded nanofibers and gold precursor. After immobilizing glucose oxidase onto the composite, the biohybrid system could be used as a component of a biosensor for investigating bio-electrochemical activity (Scheme 1). This is the first time that this hybrid structure has been used as molecular wires between the enzyme and electrode to facilitate directed electron transfer in biological sensing.

2. Experimental

2.1 Materials

The basic chemicals used in the research, triblock poly(ethylene oxide)-*b*-poly(propylene oxide)-*b*-poly(ethylene oxide), PEO-PPO-PEO, copolymer Pluronic P123 (EO20PO70EO20)

and poly(allylamine hydrochloride) (PAH) were received from Alfa Aesar company; polyvinylpyrrolidone (PVP) was delivered from Aldrich; and glucose oxidase (GOx, EC.1.1.3.4, TYPEVII, 150 U mg^{-1}) was purchased from Fluka. Other chemicals were purchased from Shanghai Chemical Co., Ltd. All chemicals were used as received, without further treatment.

2.2 Preparation of spinning sols

The first step in the silica fiber preparation was to generate silicate spinning sol. In a typical synthesis (similar to Wang *et al.*),[45] 1.0 g P123, 2.36 g PVP (Mw = 1 300 000), and 3.0 g TEOS were dissolved in 20 g absolute alcohol, and then 2 M HNO_3 in the amount of 0.2 g was added dropwise as a catalyst. The mixture was vigorously stirred at room temperature to be perfectly dissolved. After refluxing at 80 °C for 0.5 h under constant stirring, the homogenous solution was aged at 80 °C for 24 h to form sol precursor with a viscosity of 1100 mPa s.

2.3 Electrospinning

In the process of silica nanofiber production, 3 mL of spinning sol was transferred to a 5 mL syringe attached to a 25 gauge stainless steel needle. Then the needle was electrified using a high-voltage DC supply (DWX-P403-0.2FD4, Dongwen High Voltage, Tianjin, China) and voltage of 10 kV was applied. The spinning sol was pushed through the needle tip at a rate of 3 mL h^{-1} with the help of a syringe pump (ALC-IP 900, Alcott Biotech CO. LTD, Shanghai, China). The receiving electrode was a grounded copper mesh at a distance of 20 cm from the needle tip. The fibers collected on the copper mesh were left overnight at 40 °C to hydrolyze, and then they were calcined in a muffle, which was heated from room temperature to 550 °C at a rate of 2 °C min^{-1}. Calcination was carried out in air for 2 h.

2.4 PAH-Functionalization of silica nanofibers and gold seed attachment

The layer-by-layer (LbL) self-assembled method was adopted to sequentially absorb PAH and $AuCl_4^{-1}$ onto the fiber surface. Typically, 40 mg calcined fibers were soaked in 60 mL of 2 g L^{-1} PAH solution. After dispersion by sonication, the solution was left standing for 48 h at room temperature, and then centrifuged. The precipitate was washed twice with deionized water. The obtained PAH-modified fibers were immersed in 10 mL of 1.71 mM $HAuCl_4$ aqueous solution for 24 h to combine $AuCl_4^{-1}$ with $-CH_2NH_3^+$ group *via* electrostatic attraction. Centrifuged and washed twice, the resulting modified fibers were redispersed in 0.1 M $NaBH_4$ solution for reduction of $AuCl_4^{-1}$. The color of the suspension rapidly changed from buff to red wine, indicating the formation of gold seeds on the fiber surface. The functionalized fibers were obtained by centrifugation and washing twice with deionized water.

2.5 Growth of gold nanoshell

To grow into shell on the modified fibers surface, 8.55 g PVP K30 (M_w = 40 000) was dissolved in 30 mL ethylene glycol (EG) to result in 6.71 mM solution. After the mixture was stirred for homogenization, solution was injected into a 3-neck flask (fitted with a reflux condenser and a teflon-coated stir bar) and heated in air at 70 °C for 30 min. The fibers carrying gold seeds were then added to the EG and heated for an additional 30 min. Subsequently, 7.06 mM $HAuCl_4$ (0.034 g) was prepared in 12.40 mL of EG at room temperature and added dropwise into the flask over a period of 10 min. The reaction mixture was heated at 70 °C for another 2, 3, 5, and 10 h to control the thickness of gold shell. The final product was washed thoroughly with ethanol and water to remove EG and excess PVP. It is noted that herein the molar ratio of PVP K30 repeating units to $AuCl_4^-$ ions, R, was *ca.* 908. In order to investigate the effect of R value on the shell morphology, under the condition of R = 405, the gold nanoparticles were also synthesized in absence of fibers supporting gold seeds.

2.6 Immobilization of GOx and bioelectrochemical measurements

Commercial indium tin oxide on glass (ITO; resistivity < 15 Ω) was used as the substrate for electrode buildup, which was cleaned by sonication sequentially for 20 min each in acetone, 10% KOH in ethanol and doubly deionized water. After the treatment, a certain amount of fiber suspension (5 mg final fibers were dispersed in 1 mL 0.2 M phosphate buffer solution; PBS pH 6.8), 0.05 M L-cysteine water solution, 10% glutaric dialdehyde aqueous solution, 5 mg mL^{-1} GOx solution (in 0.1 M phosphate buffer; PBS pH 6.8) were sequentially dropped on cleaned electrode surface (for details of fabrication refer to Scheme 1). The modied ITO (denoted as fibers-2/ITO, fibers-3/ITO, fibers-5/ITO, fibers-10/ITO, respectively, according to the coating time of gold shell) was dried with N_2 and then kept under dry condition at 4 °C.

A conventional three-electrode cell, consisting of the fibers/ITO working electrode, a platinum wire auxiliary electrode, and an Ag/AgCl (3 M KCl) reference electrode, was used for the electrochemical measurements. All potentials are reported with respect to the SCE. Cyclic voltammetry measurements were performed at room temperature (25 °C) using a CHI 660C (CH Instruments, Chenhua, Shanghai, China) connected to a personal computer.

2.7 Characterization

The assembly of PAH and $AuCl_4^{-1}$ onto the fiber surface was verified by MAlVERN 3000 HS Zetasizer. To demonstrate the overall uniformity and morphology of the particles, the samples were examined by scanning electron microscopy (SEM) using a JEOL SM-6360LV microscope equipped with an energy dispersive X-ray analyzer (EDX). The average diameter of core-shell fibers was determined from SEM images measuring 100 different fiber segments selected over 5 fields of view. For high-resolution images, all samples were placed on a carbon-coated copper grid and dried at room temperature overnight. To enhance the electrical conductivity, the samples were coated with carbon *via* sputtering. Higher resolution images were obtained by transmission electron microscopy (TEM) using a HITACHI H-200 TEM instrument at an accelerating voltage of 200 kV. The samples for TEM micrographs were prepared by embedding the fibers into a resin and

microtoming the resin into 100 nm thick slices. All TEM samples were deposited on 300 mesh Holey carbon-coated copper grids and dried overnight before examination. The crystalline structure of Au shell was investigated by X-ray power diffraction (RIGAK, D/MAX 2550 VB/PC, Japan) and solid-state UV-Vis reflectance spectrophotometer (UV-Vis, Shamadzu UV-2450 spectrometer, 200–800 cm^{-1} wavelength) respectively. To confirm the mesoporous structure, the silica fibers were analyzed using the N_2 sorption characterization method (Micromeritics ASAP 2010).

3. Results and discussion

In the research, suitable silica fibers play a key role in fabricating an excellent biohybrid system, so it is necessary to first investigate the properties of silica fibers. The detailed measurements are as follows.

Fig. 1 shows the morphology of silica fibers before and after calcination. Obviously, the fiber diameter is significantly affected by calcination procedure, as can be seen from the comparison of Fig. 1(A) and (B). After-heated fibers present apparently smaller and more uniform diameter (about 750 nm) than non-heated fibers (diameter *ca.* 1 μm). A similar result was also reported in other studies.[45] We suggest that the dramatic volume shrinkage is related to the different roles of PVP and P123 in fibers. In this fabrication system, PVP mainly helps to shape the fibrous morphology and create the larger pores (around 15 nm) while P123 assembled into micelles so as to form smaller pores (around 5.2 nm). During calcination, PVP dramatically shrinks to bring about the volume decrease of fibers, and P123 degrades to leave the cavity corresponding to the volume of P123. Furthermore, it is noted that in our experimental procedure, the complete 3D skeleton of SiO_2 matrix is formed stepwise, that is, before calcination only silicate oligomer was generated due to the preliminary hydrolysis of TEOS, which is unable to form complete net-like structure. Only treated in high temperature, could the oligomer species be driven to further condense to SiO_2 with the release of small molecule byproducts such as ethanol and water from the fibers. This process was synchronized with the shrinkage and decomposition of PVP, which is the main reason of the dramatic volume shrinkage of the fibers. This procedure was also conformed by FT-IR spectra and DTG curve (ESI, Fig. S1 and S2†). It can be seen that, after calcinations, the characteristic peaks of Si–OH and Si–O–Si became stronger and broader because of further condensation of silica oligomer (Fig. S1, curve b), whereas the disappearance of peak of C═O (Fig. S1, curve a) in PVP molecular chain is attributable to complete degeneration or pyrolysis of PVP. Furthermore, two endothermic peaks at 190 °C and 344 °C (Fig. S2, curve a) also indicated the decomposition of P_{123} and PVP.

To specify the volume of the pores, the N_2 adsorption–desorption isotherm of the silica fibers was determined (Fig. S3, curve a). The average diameter of pore size based on BJH theory is mainly 5.2 nm, and partly 15 nm (Fig. S3, curve b). This bimodal pore size distribution was also observed from TEM micrographs (Fig. 2). It might be caused by the effect of PVP on the hydrolysis process of TEOS.[45]

In order to verify the effectiveness of self-assembly of polyelectrolyte and gold ions on the silica fiber surface, the ζ-potential at different stages of surface modification of silica fibers was measured. At pH >2, beyond the IEP (isoelectric point) of silica, the as-electrospun silica fibers are highly negatively charged due to the presence of the Si–OH groups. One layer of PAH changes the overall charge of the silica fiber surface to positive, which demonstrates successful polymer coating. Upon $AuCl_4^{-1}$-modification of the silica fibers, there is a partial loss of charge: ζ-potential falls from *ca.* 70.70 mV to *ca.* 17.90 mV. This results from the creation of ionic bonds between the $AuCl_4^{-1}$ and the $-CH_2NH_3^+$ groups of PAH. But due to the entangling conformation of PAH chains, partial positive charges of $-CH_2NH_3^+$ are embedded and cannot attract $AuCl_4^{-1}$, thus repellent force of the residual positively charged sites electrostatically stablize the silica fibers from aggregation in water. The uniform distribution of binding sites created dense and homogeneous gold nanoparticles of *ca.* 4 nm (Fig. 3(B–D)), which facilitated formation of the shell with uniform depth. It can be clearly seen that the gold nanoparticles are uniformly distributed on the fiber surface. According to Phonthammachai *et al.*'s report,[38] at pH 7, $[AuCl(OH)_3]^-$ is prevalent and optimal for surface nucleation, leading to gold crystals of smaller size and higher dispersion. This is consistent with what Fig. 3(C) and (D) show. Fig. 3A is the SEM micrograph after decorating the fiber surface with gold seeds. Differing from the smooth surface of bare silica fibers, the surface of nanoparticle–decorated fibers look rough and there are many fine particles. This further indicates that

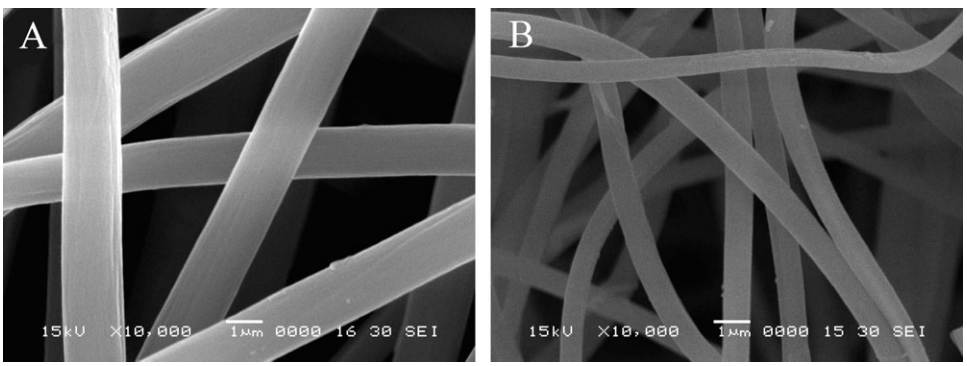

Fig. 1 SEM images of as-electrospun nanofibers before (A) and (B) after calcination treatment.

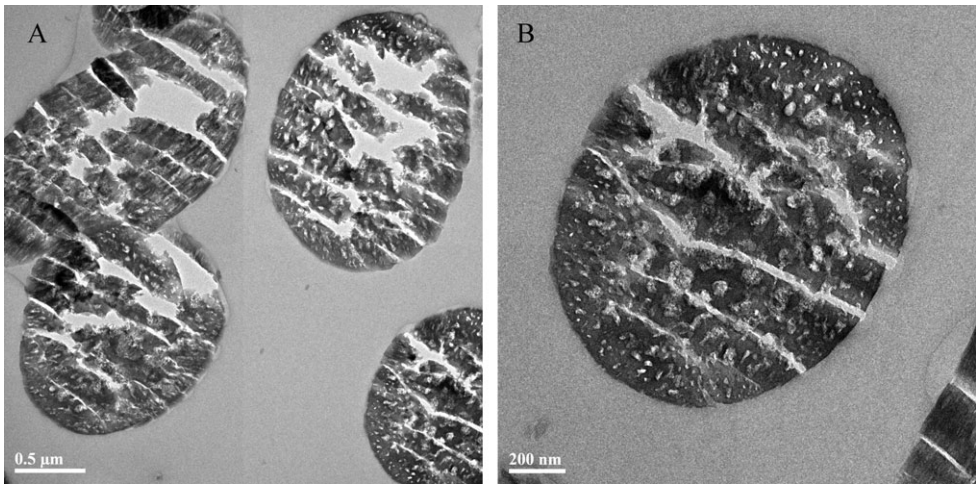

Fig. 2 Cross-section TEM images of electrospun mesoporous silica fibers. (A) 20 000× magnification and (B) higher magnification.

gold nanoparticles have been successfully absorbed on the fiber surface and polyelectrolyte coating is an effective method to control the size and distribution of nanoparticles, because the combining sites in PAH chains exclusively determine the density and quantity of gold seeds. Logar's group also used self-assembled multilayer thin films of polyelectrolytes as a template to form silver nanoparticles *in situ*.[33] It is possibly the existence of gold nanoparticles that makes the modified fibers look very dark (Fig. 3B). When a single particle is magnified in high resolution, as shown in Fig. 3D, the crystal lattice can be observed directly, with a spacing *d* of 0.24 nm. This lattice spacing corresponds to Au (111), in good agreement with literature values (JCPDS No. 04–0784), which strongly confirms the existence of metallic gold nanoparticles. EDS was used to characterize the composition of the gold seed-decorated silica nanobers (Fig. 3E). The presence of element silicon and oxygen is consistent with silica matrix. The existence of gold confirmed the successful incorporation of

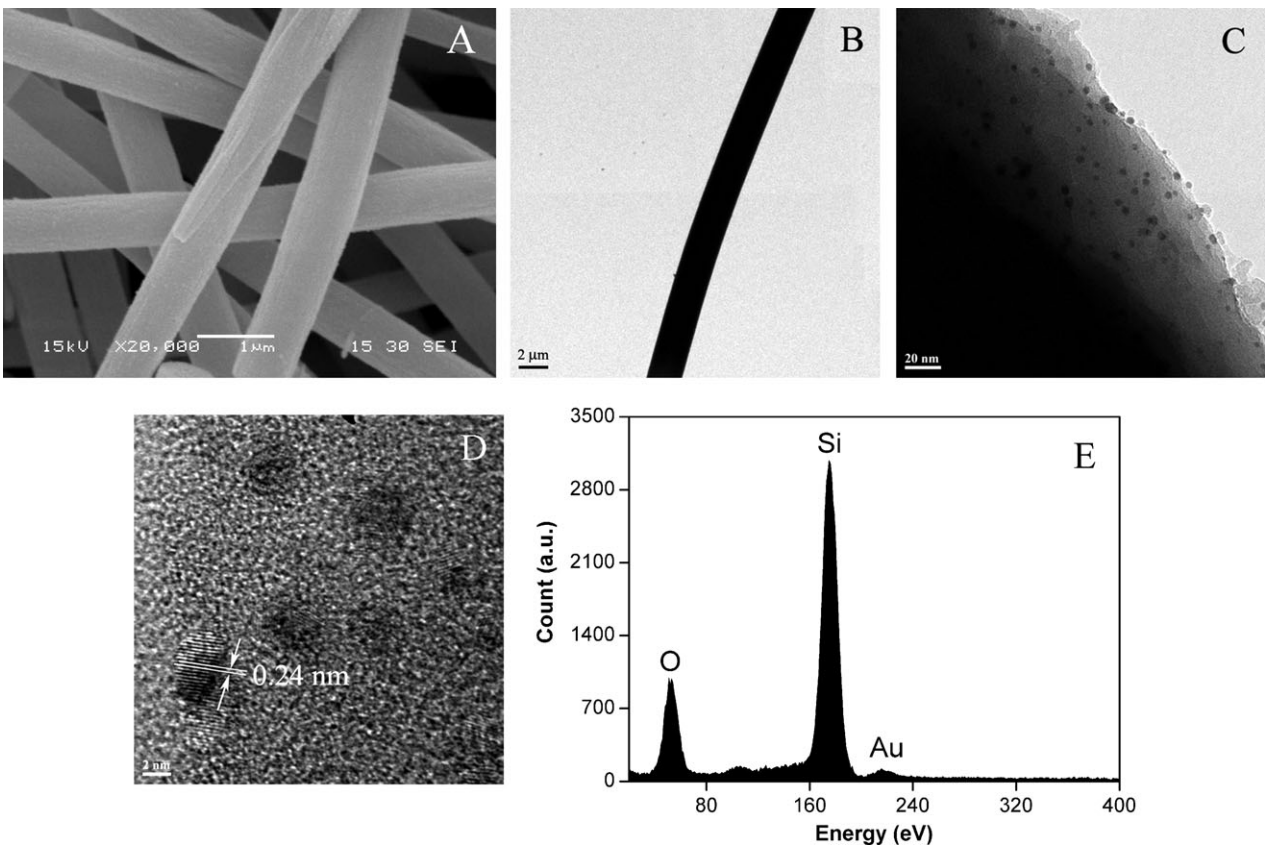

Fig. 3 (A) SEM and (B–D) TEM images and (E) EDX spectra of mesoporous silica fibers supporting gold seeds. D is a HRTEM image of an individual gold nanoparticle on fiber edge.

gold seeds onto the fiber surface. It is noted that the gold content is low, *ca.* 5.76% with respect to silica mass, suggesting the gold shell is not yet completely formed. Sodium was probably due to a residue from the sodium borohydride used for reduction.

To coat the silica nanofibers with gold in EG solution of PVP, a seeded-growth method was used in which PAH-combined seed nanoparticles act as nucleation sites. The reduction of additional gold ions in PVP solution reproducibly leads to coalescence into complete metal nanoshells. Nanoshell growth is complete within a few hours upon the extension of reductive time. PVP as a protective and reductive reagent has been extensively applied for the reduction of noble metal (such as Au, Ag) nanoparticles because of their feature of nontoxicity and good biocompatibility. However, according to a related report,[46] in the case of PVP as a reductive reagent the ratio of repeating units of vinyl pyrrolidone to gold ions could importantly impact particle size. The lower the ratio, the larger the particles. Fig. 4 shows the SEM micrograms of SiO_2@Au core-shell fibers prepared by immersing gold seed-decorated silica fibers in polyol reduction bath for 10 h (Fig. 4A) and 20 h (Fig. 4B). Under reductive conditions with the same PVP concentration, the lower the ratio (R = 405), the higher the content of gold ions. This results in not only the formation of larger particles but also the increasing of shell thickness. Fig. 4 clearly shows that the diameter of end fibers increases to *ca.* 7 μm and 12 μm after further reduction of 10 h and 20 h respectively, which is far greater than that of silica fibers. Moreover, a large amount of needle-like agglomerates was distributed on the surface and vicinity of fibers. It is considered that the agglomerates are of larger gold particles. The speculation was confirmed by Fig. S4,† *i.e.*, TEM images of gold colloid synthesized in absence of silica fibers supporting gold seeds. R is also 405 and the coating time is 5 h. It is evident that low R value and high content of gold ions favor the formation of larger particles with triangular, hexagonal, or rod-like morphology (Fig. S4(A–C)). In addition, with the increasing of reduction time, fibers partially conglutinated to form a belt structure as a result of the accumulation and coalescence of a large amount of gold nanoparticles. On the other hand, reducing reaction time also favored avoiding the formation of spicules on fiber surface (Fig. 4B). In view of this, it is necessary to optimize the R value and concentration of chloroauric acid so as to regulate the thickness of gold shell.

Fig. 5 shows SEM images of the core-shell fibers prepared by immersing the silica fibers supporting gold seeds in polyol reduction bath for 2 h, 3 h and 5 h. The value of R is 908 in the same concentration of PVP and the content of gold ions is correspondingly decreased to match R. It is clearly demonstrated that suitable R is fit for forming uniform gold shell, preventing fibers from conglutinating each other, and eliminating spicules; thus the value of R, 908, is an optimal reduction condition. It is also indicated that reaction time possibly influences the thickness and morphology of gold shell. With the time extension, more and more gold ions were reduced and absorbed on the surface of gold seeds formed at the self-assembled stage, and then gradually grew into larger particles to form continuous gold shell. The SEM images in Fig. 5 indirectly verify that reduction of short time only results in small granules rather than larger nanograins, the possible result of which is the structure of shell may be incomplete or defective. As shown in Fig. 5(A) and (B), the fibers' surfaces are smooth or only covered by dense small grains, whereas the ones in Fig. 5C seem rougher and larger grains can be seen. It is established that as long as the reduction time is suitably controlled, the thickness of gold shell will be freely tunable. The column plot of core-shell fiber diameter distribution also showed a similar trend. This method will initiate an appropriate route to synthesize various hybrids with core-shell structure, such as silica spheres coated by nano metal shell. Fig. 6 shows representative TEM images of the core-shell SiO_2@Au nanofibers coated with different depths of gold shell. It can be seen that the average thickness of gold shell basically increases with the extension of coating time. Compared with the gold-seeded fibers, no more gold particles were clearly attached to the fiber surface after the fibers were further treated for 2 h in PVP solution of chloroauric acid except that the pre-formed particles became larger. With continuing extension of the coating time, more gold particles were absorbed onto the fiber surface and combined with each other to form continuous and complete shells. The average thickness of gold shell increased from *ca.* 50, 75 to 100 nm. Moreover, after the gold seeds had further grown for 20 h, the particles began to aggregate and form irregular grains, which confirmed the results observed in Fig. S4.†

To verify the formation of gold shell, we employed X-ray diffraction (XRD, Fig. 7) and measured the powder patterns before and after forming gold shell (growing for 5 h, Fig. 5C).

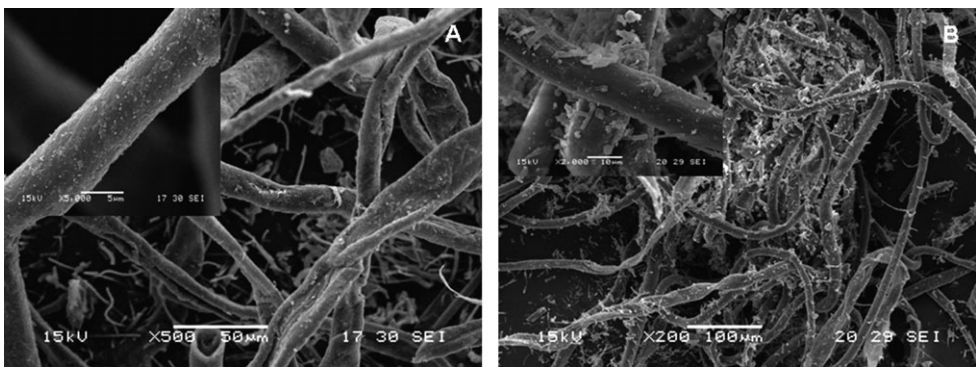

Fig. 4 SEM images of SiO_2@Au core-shell fibers prepared by immersing gold-seeded silica fibers in PVP reduction bath for (A) 10 and (B) 20 h (Inset images are locally magnified samples). The molar ratio of PVP K30 repeating units to $AuCl_4^-$ ions, R = 405.

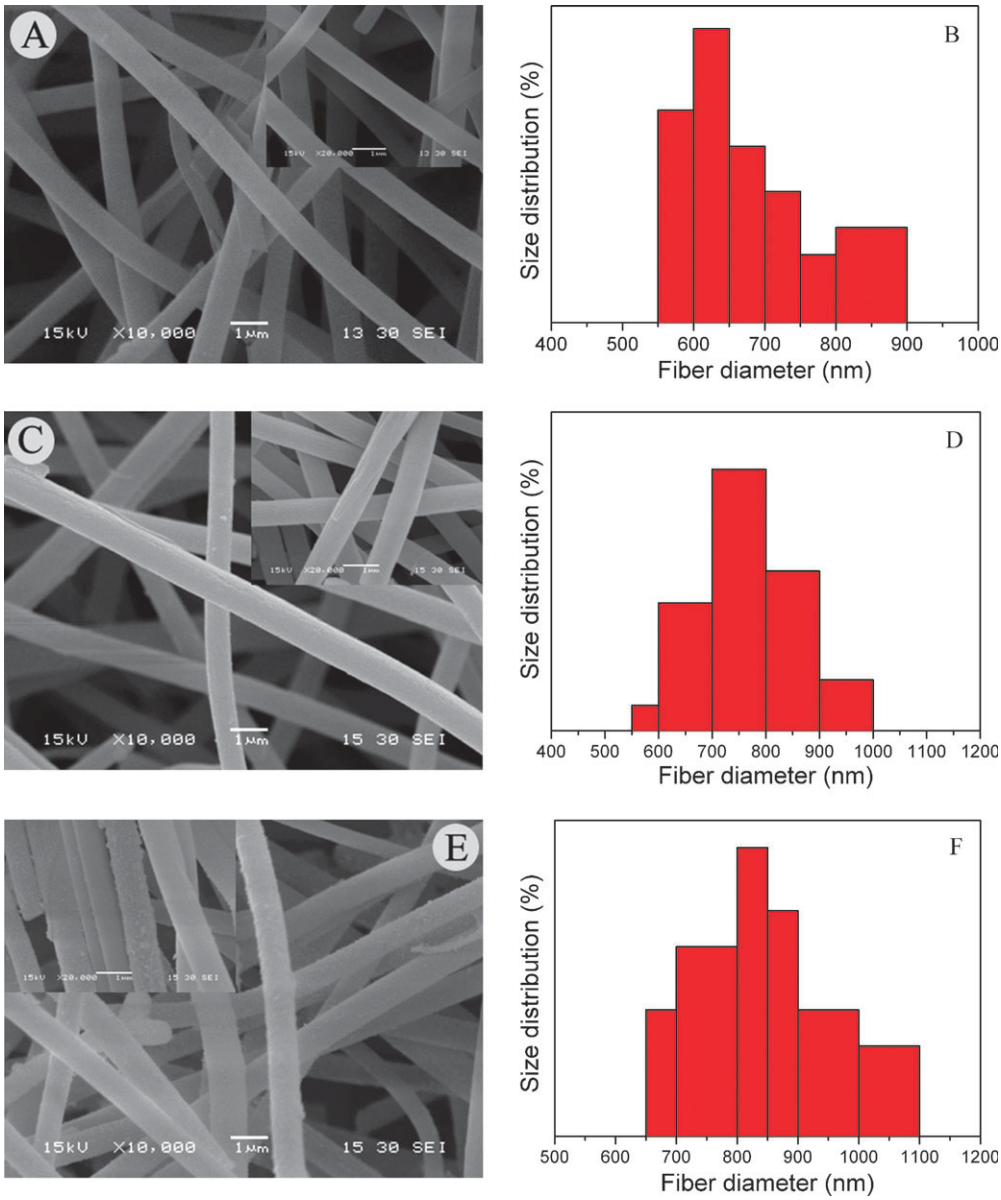

Fig. 5 SEM images (A, C, E) and column plot of diameter distribution (B, D, F) of SiO_2@Au core-shell fibers prepared by immersing gold seed-decorated silica fibers in PVP reduction bath for 2, 3, and 5 h (Inset images are locally magnified samples). The molar ratio of repeating units of PVP K30 to $AuCl_4^-$ ions, $R = 908$.

The specific XRD patterns of pure gold, characterized by three peaks positioned at 2θ values of 38.2°, 44.4°, and 64.7°, which correspond to the (111), (200), and (220) lattice planes, were not all present in both samples. The fibers carrying gold seeds only have a weak intensity peak at $2\theta = 38.2°$ which is an index of (111) lattice planes, while for the core-shell fibers, all expected diffraction peaks for the face-centered cubic structure of gold are present. It is possibly because of the low content of gold before forming complete layer that other characteristic diffraction peaks are not detected, which is in line with the findings shown in EDS analysis (Fig. 3E).

Fig. 8 shows the UV–vis spectrum of silica-fiber/gold core-shell hybrid with different thickness by varying the coating time. When a small amount of gold nanoparticles was adsorbed onto the silica fiber surface, a relatively narrow extinction peak was observed slightly red-shifted from the resonance of gold nanoparticles dispersed in aqueous solutions (520 nm). As gold nanoparticles continued growing with extending time, the extinction peak of the formed hybrid nanostructures gradually red-shifted and became broader. As more and more gold ions were reduced, the number density of gold nanoparticles gradually increased and the originally-existing seeds grew larger and larger, accordingly, the spacing between neighboring gold nanoparticles first became smaller, then more gold nanoparticles began to aggregate to form larger particles on the fiber surface. As shown in Fig. 6, the gold nanoparticles stacked so closely that they seemed to form a continuous shell. Therefore, the surface plasmon resonances of neighboring gold nanoparticles were coupled when the gap

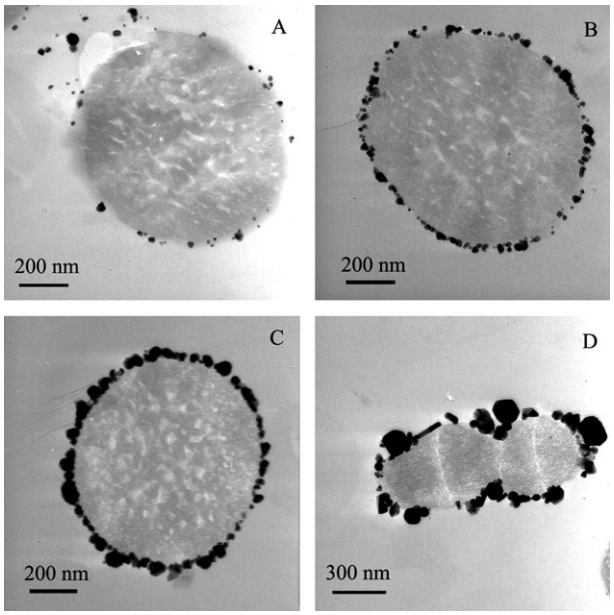

Fig. 6 Cross-section TEM images of SiO_2@Au core-shell fibers prepared by immersing gold seed-decorated silica fibers in PVP reduction bath for (A) 2, (B) 3, (C) 5 and (D) 10 h. The molar ratio of PVP K30 repeating units to $AuCl_4^-$ ions, $R = 908$.

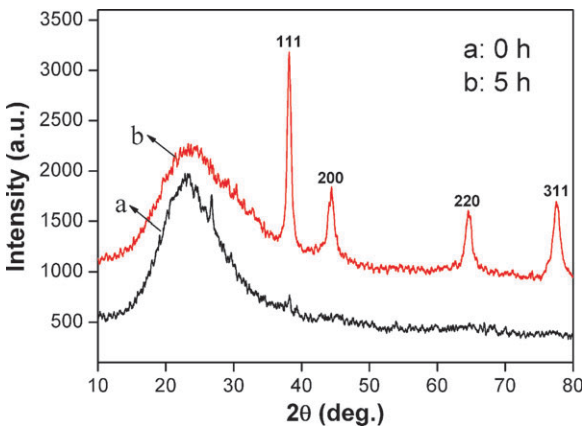

Fig. 7 XRD patterns for (a) silica fibers supporting gold seeds and (b) SiO_2@Au core-shell fibers prepared by immersing gold-seeded silica fibers in polyol reduction bath for 5 h. The molar ratio of PVP K30 repeating units to $AuCl_4^-$ ions, $R = 908$.

between the particles was comparable to the nanoparticle size. The surface plasmon coupling induced a red-shift in the surface plasmon wavelength, and this red-shift increased exponentially with decreasing nanoparticle spacing.[47] In addition, the surface-plasmon resonance of nonspherical gold nanoparticles was generally red-shifted compared to values for spherical gold nanoparticles.[48] Therefore, the red-shift and broadening (Fig. 8, curve d) of the extinction peak observed on the silica-fiber/gold hybrid core-shell nanostructures were cased by both surface plasmon coupling between closely spaced gold nanoparticles, which led to the larger and non-spherical particles. It is worth noting that only one surface-plasmon-derived extinction peak is present, suggesting that most of gold nanoparticles on the fiber surface are nearly

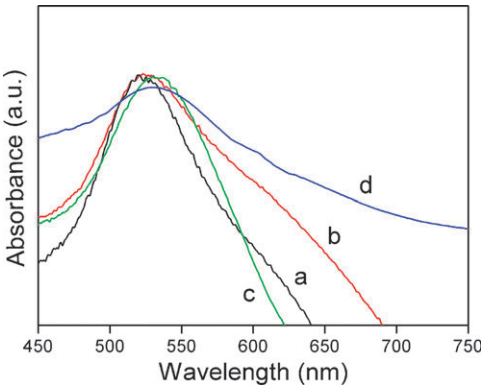

Fig. 8 Time-dependent UV-Vis spectra of SiO_2@Au core-shell fibers by immersing gold-seeded silica fibers in PVP reduction bath for (a) 2, (b) 3, (c) 5 and (d) 10 h. The molar ratio of PVP K30 repeating units to $AuCl_4^-$ ions, $R = 908$.

spherical. Therefore, although the silica fibers are one-dimensional in structure, they do not show the two characteristic surface plasmon extinction peaks as gold nanorods.[49] This is possibly ascribable to the effect of R, which appropriately controlled the morphology of gold nanoparticles. It is also inferred that nonspherical gold nanoparticles which typically have surface plasmon resonance extinction peaks more than one should be synthesized by tuning the value of R (Fig. S4†). Moreover, the local electric-field enhancement at the surface plasmon wavelength was generally larger for nonspherical nanoparticles.[50] These properties can be expected to find interesting applications in the area of photonics and optoelectronics. The diverse properties of multi-components are greatly influenced by the types of components, particle sizes, surface geometries, and distance between the nanoparticles. On the basis of these factors, gold-based systems can provide unique electrically conductive properties. For example, these hybrid nanostructures are therefore potentially useful for ultrasensitive chemical or biological sensing as intermedia enhancing electron transmission because of their excellent biocompatibility and electric conductivity.

Gold nanoparticles exhibit unique or improved electronic and optical properties. They can be easily modified using a wide range of biomolecules or chemical ligands and also facilitate electron transfer[51], which make them become one of the most promising materials to fabricate high performance biosensors. Tang's group[52] introduced gold nanorods to enhance the current response of choline biosensors. The largest responding current is up to 0.2 mA, and detection limitation is 2×10^{-5} to 4×10^{-4} M. Chen's group[53] used chitosan as a matrix for gold nanoparticle (GNP) formation and immobilization by a simple and controllable electrodeposition method. The electroactive GNPs were effectively incorporated into the chitosan hydrogel to form a biocomposite sensing film which was further used for the fabrication of non-enzyme glucose biosensor. The results show that this biocomposite film could provide plenty of active sites for direct oxidation of glucose and prepared sensor exhibited high performance. The largest responding current is up to 0.05 mA, and the detective limitation is 3.70×10^{-4} M.

Although gold nanoparticles have been proverbially applied in various biohybrid systems, the electron transmission mainly depends on conformation and morphology of GNPs. Contact between GNPs and the electrode surface is an important determinant. It is well known that the electrical contacting of redox enzymes with electrodes is the fundamental pre-requisite for the development of bioelectronic systems, such as electrochemical biosensors or biofuel cell elements.[54] Therefore, trying to decrease the electron transfer resistance between electrode surface and bioactive molecules is of first importance. One-dimensional fibrous structure has more advantages over the zero-dimensional spherical GNPS in electron transfer due to their perfect network and high surface-to-volume ratio. They can facilitate electron transfer from the redox centre of a protein, as a high volume molecule, to the electrode surface *via* the interconnected conductive paths of fibrous structure. Zhang *et al.*[55] found that the electron transfer ability of CuO nanowires was stronger than that of CuO nanoplatelets. However, more attention has not been paid to gold nanoparticle/silica core-shell fibers hybrids with high ratio, especially the ones with a continuous gold layer, used as building blocks to fabricate biosensors.

Fig. 9 shows the cyclic voltammograms of electrodes modified by core-shell fibers with different thickness of gold layer for sensitive detection of glucose. At the hybrid modified electrodes, the immobilized GOx showed direct electrochemical response. A couple of stable and well-defined redox peaks were observed. The peak-to-peak separation between the cathodic and anodic peak potential is 320 mV at scan rate of 100 mV s^{-1}. This suggests that the electrochemical process of GOx immobilized in hybrid network on fibers/ITO modied electrode is quasi-reversible.

With the increase of the gold shell thickness, the anodic current of the direct electrochemistry increased significantly and the cathodic current decreased slightly, which demonstrated an electrocatalytic oxidation process of glucose by the bioconjugated GOx, and that the hybrid composite shuttled efficiently electron between the bioactive center of GOx and electrode surface. It is a signal, on the other hand, that long reaction time favors the full growth of gold shell which facilitates electron transfer *via* electric wire built on three-dimensional network of fibers instead of the electronic

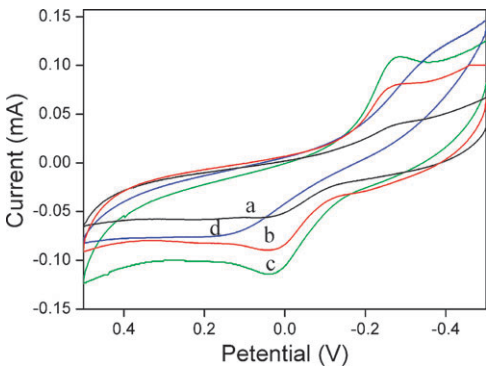

Fig. 9 Cyclic voltammograms of (a) fibers-2/ITO, (b) fibers-3/ITO, (c) fibers-5/ITO and (d) fibers-10/ITO at 0.1 V s^{-1} scan rate. Data were recorded in 0.10 M phosphate buffer (pH 6.8) that included 11 mmol glucose at room temperature.

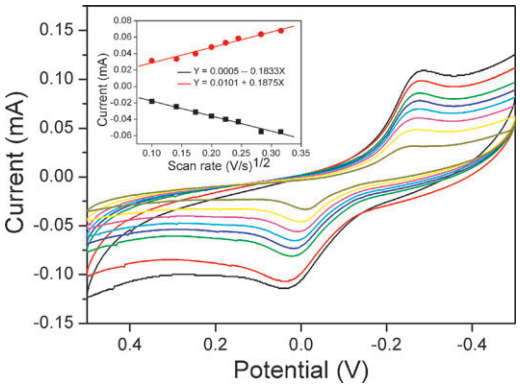

Fig. 10 Cyclic voltammograms of fibers-5/ITO in 0.1 M PBS buffer solution (pH 6.8) at different scan rates: 10, 20, 30, 40, 50, 60, 80 and 100 mV s^{-1}, respectively (from inner to outer). Data were recorded in 0.10 M phosphate buffer (pH 6.8) that included 11 mmol glucose at room temperature.

hopping between neighboring gold nanoparticles. Meanwhile, the electrode modified with silica-fiber/gold core-shell hybrid shows a high electrocatalytic current towards the oxidation of glucose compared with the reported AuNPs-SBA-15/GOx modified electrode,[56] which is the benefits of a three-dimensional distribution of enzyme molecules bioconjugated with fibers.[57] However, the gold-seeded silica fibers treated for 10 h in PVP solution of chloroauric acid did not show superior electrocatalytic capability (Fig. 9d). We surmise that those large gold particles with irregular morphology scattering on the hybrid surface may seriously deteriorate the integrity of gold shell, thus decreasing the efficiency of electron transfer.

The effect of the scan rate (ν) on the peak currents (i_{pa} and i_{pc}) has been investigated in the range of 10–100 mV s^{-1}. Fig. 10 shows the CVs of the electrode denoted as fibers-5/ITO modified by gold nanofiber/silica hybrid with the shell growing for 5 h at different scan rates in the potential range of −0.5 to +0.5 V in pH 6.8 PBS. As shown in the figure, peak currents and difference between peak potentials increase with the scan rate increasing. The inset of Fig. 10 shows that the relationship between peak currents and the square root of scan rates for the redox reaction of GOx are linear. At low scan rate (<80 mV s^{-1}), the cathodic and anodic peak currents were directly proportional to the square root of scan rate (mV). The regression equations are: i_{pc} (mA) = 0.01007 + 0.18753ν (mV s^{-1}) with correlation coefficient 0.9876 and i_{pa} (mA) = 0.00058 − 0.1833ν (mV s^{-1}) with correlation coefficient 0.9909, indicating that the electrode process is a surface-controlled process. Other possible causes are the resistance of the material or an electron transfer process initiated by an electro-hopping mechanism.[58] These findings suggest that the GOx has been successfully adsorbed onto the hybrid fiber surface.

4. Conclusions

In this study, mesoporous silica-fiber/gold core-shell nanostructure has been successfully synthesized. Electrospun mesoporous silica fibers were used as templates for the assembly of gold nanoparticles and the formation of continuous gold

shells along the fiber axis. Dense and uniform spherical gold nanoparticles were formed by *in situ* reduction of hydrochloroauric acid absorbed on self-assembled polyelectrolyte film of silica fiber surface. The gold-seeded silica fibers were further coated by continuous gold shells *via* solution-phase reduction of an appropriate metal ion in PVP solution. The thickness and morphology of gold shell could be tailored by the molar ratio of repeating units of PVP to gold ions (R) and growth time. Silica-fiber/gold core-shell hybrid nanostructures exhibit extinction spectra different from the spectra of gold colloid in solution, and were further used as building blocks for fabrication of glucose biosensor, which exhibited excellent bio-electrochemical activity with high sensitivity and rapid response. These hybrid nanostructures can be, therefore, used as electron transfer mediator to enhance the electron transition in ultrasensitive chemical or biological sensor. By functionalizing the mesopores in fibers, potential applications will be further exploited.

Acknowledgements

This work was supported by the National Natural Science Foundation of China (20676038, 20976054), the Key Project of Science and Technology for Ministry of Education (107045), the Innovation Program of Shanghai Municipal Education Commission (09ZZ58), the Program of Shanghai Subject Chief Scientist (08XD1401500), the Shuguang Scholar-Tracking Foundation of Shanghai (08GG09), and the Shanghai Leading Academic Discipline Project (B502).

Notes and references

1 D. A. Ferrer, L. A. Diaz-Torres, S. M. Wua and M. Jose-Yacaman, *Catal. Today*, 2009, **147**, 211.
2 Y. M. Zhai, J. F. Zhai, Y. L. Wang, S. J. Guo, W. Ren and S. J. Dong, *J. Phys. Chem. C*, 2009, **113**, 7009.
3 W. Zhang, L. Li, Y. K. Du, X. M. Wang and P. Yang, *Catal. Lett.*, 2009, **127**, 429.
4 D. X. Li, Q. He and J. B. Li, *Adv. Colloid Interface Sci.*, 2009, **149**, 28.
5 C. H. Liang, C. Chung and Y. Wu, *Anal. Chem.*, 2009, **81**, 7750.
6 P. Zhang, J. Cai, Y. X. Chen, Z. Q. Tang, D. Chen, J. L. Yang, D. Y. Wu, B. Ren and Z. Q. Tian, *J. Phys. Chem. C*, 2010, **114**, 403.
7 M. A. Nash, J. J. Lai, A. S. Hoffman, P. Yager and P. S. Stayton, *Nano Lett.*, 2010, **10**, 85.
8 W. Xie, L. Su, P. Donfack, A. G. Shen, X. D. Zhou, M. Sackmann, A. Materny and J. M. Hu, *Chem. Commun.*, 2009, 5263.
9 R. Costi, A. E. Saunders, E. Elmalem, A. Salant and U. Banin, *Nano Lett.*, 2008, **8**, 637.
10 E. Formo, E. Lee, D. Campbell and Y. N. Xia, *Nano Lett.*, 2008, **8**, 668.
11 K. Awazu, M. Fujimaki, C. Rockstuhl, J. Tominaga, H. Murakami, Y. Ohki, N. Yoshida and T. Watanabe, *J. Am. Chem. Soc.*, 2008, **130**, 1676.
12 J. S. Lee, E. V. Shevchenko and D. V. Talapin, *J. Am. Chem. Soc.*, 2008, **130**, 9673.
13 A. Wijaya, S. B. Schaffer, I. Pallares and G. K. Hamad-Schifferli, *ACS Nano*, 2009, **3**, 80.
14 D. Pissuwan, S. M. Valenzuela, C. M. Miller and M. B. Cortie, *Nano Lett.*, 2007, **7**, 3808.
15 W. Eck, G. Craig, A. Sigdel, G. Ritter, L. J. Old, L. Tang, M. F. Brennan, P. J. Allen and M. D. Mason, *ACS Nano*, 2008, **2**, 2263.
16 W. H. Ni, Z. Yang, H. J. Chen, L. Li and J. F. Wang, *J. Am. Chem. Soc.*, 2008, **130**, 6692.
17 C. Z. Li, K. B. Male, S. Hrapovic and J. H. T. Luong, *Chem. Commun.*, 2005, 3924.
18 C. G. Wang and J. Irudayaraj, *Small*, 2008, **4**, 2204.
19 G. Y. Liu, H. F. Ji, X. L. Yang and Y. M. Wang, *Langmuir*, 2008, **24**, 1019.
20 P. Wang, Y. H. Zhu, X. L. Yang, C. Z. Li and H. L. Du, *Acta Mater.*, 2008, **56**, 1144.
21 A. C. Patel, S. Li, C. Wang, W. J. Zhang and Y. Wei, *Chem. Mater.*, 2007, **19**, 1231.
22 J. G. Lee, J. C. Park, J. U. Bang and H. J. Song, *Chem. Mater.*, 2008, **20**, 5839.
23 Y. Y. Song, X. B. Cao, Y. Guo, P. Chen, Q. R. Zhao and G. Z. Shen, *Chem. Mater.*, 2009, **21**, 68.
24 L. M. Liz-Marzán, M. Giersig and P. Mulvaney, *Langmuir*, 1996, **12**, 4329.
25 H. B. Lee, Y. M. Yooa and Y. H. Hanb, *Scr. Mater.*, 2006, **55**, 1127.
26 S. M. Kang, K. B. Lee, D. J. Kim and I. S. Choi, *Nanotechnology*, 2006, **17**, 4719.
27 Y. L. Shi and T. Asefa, *Langmuir*, 2007, **23**, 9455.
28 J. Xu and C. C. Perry, *J. Non-Cryst. Solids*, 2007, **353**, 1212.
29 Y. l. Qi, M. Chen, S. Liang, J. Zhao and W. Yang, *Colloids Surf., A*, 2007, **302**, 383.
30 J. G. Xue, C. G. Wang and Z. F. Ma, *Mater. Chem. Phys.*, 2007, **105**, 419.
31 F. Caruso, H. Lichtenfeld, M. Giersig and H. Möhwald, *J. Am. Chem. Soc.*, 1998, **120**, 8523.
32 X. Hong, J. Li, M. J. Wang, J. J. Xu, W. Guo, J. H. Li, Y. B. Bai and T. Li, *Chem. Mater.*, 2004, **16**, 4022.
33 M. Logar, B. Jančar, D. Suvorov and R. Kostanjšek, *Nanotechnology*, 2007, **18**, 325601.
34 V. Salgueiriño-Maceira, M. A. Correa-Duarte, M. Farle, A. López-Quintela, K. Sieradzki and R. Diaz, *Chem. Mater.*, 2006, **18**, 2701.
35 S. Z. Zhang, W. H. Ni, X. S. Kou, M. H. Yeung, L. D. Sun, J. F. Wang and C. H. Yan, *Adv. Funct. Mater.*, 2007, **17**, 3258.
36 Y. Q. Qu, R. Porter, F. Shan, J. D. Carter and T. Guo, *Langmuir*, 2006, **22**, 6367.
37 Y. Yang, M. Hori, T. Hayakawa and M. Nogami, *Surf. Sci.*, 2005, **579**, 215.
38 N. Phonthammachai, J. C. Y. Kah, G. Jun, C. J. R. Sheppard, M. C. Olivo, S. G. Mhaisalkar and T. J. White, *Langmuir*, 2008, **24**, 5109.
39 M. Wang and N. Pan, *Mater. Sci. Eng., R*, 2008, **63**, 1.
40 M. Wang, N. Pan, J. K. Wang and S. Y. Chen, *J. Colloid Interface Sci.*, 2007, **311**, 562.
41 L. W. Ji, Z. Lin, A. J. Medford and X. W. Zhang, *Chem.–Eur. J.*, 2009, **15**, 10718.
42 C. C. Kuo, Y. C. Tung and W. C. Chen, *Macromol. Rapid Commun.*, 2010, **31**, 65.
43 H. S. Yoo, T. G. Kim and T. G. Park, *Adv. Drug Delivery Rev.*, 2009, **61**, 1033.
44 J. Hana, T. X. Chena, C. J. Branford-Whiteb and L. M. Zhu, *Int. J. Pharm.*, 2009, **382**, 215.
45 Y. Y. Zhao, H. Y. wang, X. F. Lu, X. Li, Y. Yang and C. Wang, *Mater. Lett.*, 2008, **62**, 143.
46 C. E. hoppe, M. Lazzari, I. Paradiñas-Blanco and M. A. López-Quintela, *Langmuir*, 2006, **22**, 7027.
47 K. H. Su, Q. H. Wei, X. Zhang, J. J. Mock, D. R. Smith and S. Schultz, *Nano Lett.*, 2003, **3**, 1087.
48 C. K. Tsung, X. S. Kou, Q. H. Shi, J. P. Zhang, M. H. Yeung, J. F. Wang and G. D. Stucky, *J. Am. Chem. Soc.*, 2006, **128**, 5352.
49 H. Y. Koo, W. S. Choi and D. Y. Kim, *Small*, 2008, **4**, 742.
50 K. L. Kelly, E. Coronado, L. L. Zhao and G. C. Schatz, *J. Phys. Chem. B*, 2003, **107**, 668.
51 J. Wang and M. Musameh, *Anal. Chem.*, 2003, **75**, 2075.
52 X. L. Ren, F. Q. Tang, R. Liao and L. Zhang, *Electrochim. Acta*, 2009, **54**, 7248.
53 D. Feng, F. Wang and Z. L. Chen, *Sens. Actuators, B*, 2009, **138**, 539.
54 Y. M. Yan, R. Tel-Vered, O. Yehezkeli, Z. Cheglakov and I. Willner, *Adv. Mater.*, 2008, **20**, 2365.
55 X. J. Zhang, G. F. Wang, X. W. Liu, J. J. Wu, M. Li, J. Gu, H. Liu and B. Fang, *J. Phys. Chem. C*, 2008, **112**, 16845.
56 Y. Bai, H. Yang, W. W. Yang, Y. C. Li and C. Q. Sun, *Sens. Actuators, B*, 2007, **124**, 179.
57 Y. P. Shana, G. C. Yang, J. Gong, X. L. Zhang, L. D. Zhu and L. Y. Qua, *Electrochim. Acta*, 2008, **53**, 7751.
58 S. Rezaei-Zarchi, A. A. Saboury, P. Norouzi, J. Hong, S. Ahmadian, M. R. Ganjali, A. A. Moosavi-Movahedi, A. B. Moghaddam and A. Javed, *J. Appl. Electrochem.*, 2007, **37**, 1021.